Peer-reviewed version available at Atoms 2018, 6, 44; doi:10.3390/atoms6030044

Research Article

Measurement of electron density from Stark-broadened nanomaterial plasma

Ashraf M. EL Sherbini [1], Ahmed E. EL Sherbini [2], and Christian G. Parigger [3,*]

[1] Laboratory of Laser and New Materials, Faculty of Science, Cairo University, Giza, Egypt; elsherbinia@sci.cu.edu.eg
[2] Laboratory of Laser and New Materials, Faculty of Science, Cairo University, Giza, Egypt; ahmed.azdakyne@gmail.com
[3] Department of Physics and Astronomy, University of Tennessee/University of Tennessee Space Institute, 411 B. H. Goethert Parkway, Tullahoma, TN – 37388, USA; cparigge@tennessee.edu
* Correspondence: cparigge@tennessee.edu; Tel.: +1-931-841-5690

Abstract: This work communicates results from optical emission spectroscopy following laser-induced optical breakdown at or near nanomaterial. Selected atomic lines of silver are evaluated for consistent determination of electron density. Comparisons are presented with Balmer series hydrogen results. Of particular interest are measurements free of self-absorption effects. For several silver lines, asymmetries are observed in the recorded line profiles. Electron densities of interest range from 0.5 to 3 × 10^{17} cm^{-3}, for 5 nanosecond Q-switched Nd:YAG radiation at wavelengths of 1064, 532, and 355 nm, and for selected silver emission lines including 328.0, 338.2, 768.7, and 827.3 nm, and the hydrogen alpha Balmer series line at 656.3 nm. Line asymmetries are presented for the 328.0 nm Ag I line that is measured following generation of the plasma due to multiple photon absorption. This work explores electron density variations for different irradiance levels, and reports spectral line asymmetry of resonance lines for different laser fluence levels.

Keywords: Laser-induced plasma; Stark broadening; electron density; nanomaterial; atomic spectroscopy; silver; hydrogen;

1. Introduction

Laser-induced breakdown spectroscopy (LIBS) [1] is utilized for the measurement of plasma generated at or near silver nanomaterial. During the last few decades, LIBS has been recognized for its versatility and integral aspect for a variety of spectro-chemical analysis procedures. Typically, high peak power, nominal nanosecond radiation is focused to irradiance levels of the order of a few MW/cm^2 to TW/cm^2, and the emitted light is analyzed with spectrometers and usually gated array detectors [2, 3]. Historically, laser-induced plasma spectroscopy (LIPS) explores the physics of the plasma induced by laser light via optical emission spectroscopy (OES) [4, 5, 6, 7]. Spectral line shape analysis via OES leads to determination of at least one characteristic plasma parameter, namely, electron density, n_e.

The measurement of electron density is of prime importance for description of the plasma induced by laser radiation. Spectroscopically, n_e can be measured using different experimental techniques that include: measurement of the optical refractivity of the plasma [4, 5, 6, 7], calculation of the principal quantum number at the series limit [4, 5, 6, 7], measurement of the absolute emission coefficient (spectral intensity in Watt/ m^3 sr) of a spectral line [8], and measurement of the absolute emissivity of the continuum emission (Watt/ m^3 sr) [8]. However, measurement of Stark broadening of emitted lines for n_e determination has been the widely utilized [4, 5, 6, 7, 8].

Peer-reviewed version available at Atoms 2018, 6, 44; doi:10.3390/atoms6030044

Measurements of n_e from Stark-broadening is relatively straightforward provided that the Stark effect is the dominant broadening mechanism, with significantly smaller contributions from Doppler broadening and other pressure broadening mechanisms resulting from collisions with neutral atoms (i.e., resonance and Van der Waals broadening) [4, 5, 6, 7]. Theoretical calculations of Stark broadening parameters of hydrogen and hydrogenic lines are communicated by H. Griem [4] and E. Oks [9, 10, 11]. Precise fitting of the measured line shapes to convolutions of Lorentzian and Gaussian spectral line shapes - Voigt function – allows one to extract the Stark full width at half maximum (FWHM). Subsequently, the electron density can be inferred from tabulated Stark broadening tables.

2. Nanomaterial

Nanomaterials usually describe structured components with at least one dimension less than 100 nm [12]. Two principal factors cause the properties of nanomaterials to differ significantly from bulk materials, namely, the increase in the relative surface area and the quantum effects. These factors can substantially change and/or enhance the well-known bulk properties, such as chemical reactivity [13], mechanical strength [14], electrical and magnetic [15], and optical characteristics [16]. As the particle size decreases, a greater proportion of atoms are found at the surface than in the interior [17]. The quantum effects can begin to dominate the properties of matter as its size is reduced to the nano-scale. Nanoparticles are of interest because of its inherent new properties when compared with larger particles of the same materials [12, 13, 14, 15, 16, 17].

It was found that the addition of thin layer of gold and silver nanoparticles to the surface of analyte matrix alloys lead to signal improvement, and hence an improved limit of detection (LOD) in LIBS applications [18]. The acronym associated with improved emission signals is Nano-Enhanced Laser Induced Breakdown Spectroscopy (NELIBS). Conversely, interaction of high peak power radiation with pure nanomaterial targets [19, 20, 21, 22] is investigated with so-called Nano-Enhanced Laser Induced Plasma Spectroscopy (NELIPS).

In previous NELIPS work, the signal enhancement shows the following trends: (1) the enhanced emission from the nanomaterials increases linearly with time delays when compared with bulk material [19]; (2) the enhanced emission increases with decreasing laser fluence [20]; (3) there are no apparent changes of the plasma electron density and temperature[21, 22] ; (4) the enhancement factors that may vary for different experimental conditions can be associated with the relative masses ejected from the targets [21, 22]; (5) The threshold of the plasma ignition from the surface of the nanomaterials is much smaller than that from the corresponding bulk [21, 22]; (6) the breakdown threshold is inversely proportional to the square of the incident laser wavelength [20, 21, 22]; and finally (7) the threshold of the plasma from the nano-material targets changes linearly with the diameter size of the nanoparticles [22].

Moreover, the modeling of the laser-induced plasma from either type of targets (Bulk and Nano) has been theoretically investigated after the addition of a laser wavelength dependent term [21, 22] which was found to contribute of the order of 90 per cent when using near UV laser wavelengths [21, 22].

3. Materials and Methods

This work utilizes the same experimental setup reported in previous articles [21, 22]. It comprises a Nd-YAG laser device (type Quantel-Brilliant B) operated at the fundamental wavelength of 1064 nm and two higher harmonics at 532 and 355 nm with output laser energy of 30±3, 100±4, and 370±5 mJ, respectively. The focusing lens was located at a distance about 95±1 mm, away from the target material. Using a special thermal paper (supplied by Quantel®), a circular laser beam spot revealed

Peer-reviewed version available at Atoms 2018, 6, 44; doi:10.3390/atoms6030044

a radius of 0.27 ± 0.03 mm. In order to avoid laser focusing-lens chromatic aberrations, the plasma initiation was first observed in laboratory air, and subsequently, the target was displaced closer to the 100 mm focal-length achromatic lens. This routine would indicate that the plasma emission originated from the target rather than from ambient air surrounding the target. The light from the plasmas was collected using a 400 μm diameter optical fiber (with numerical aperture NA=0.22) to the entrance slit of the SE200-Echelle type spectrograph (with optical resolution of 0.02 nm per pixel with an average instrumental bandwidth of 0.2 nm). The optical fiber was positioned at distance of 5 mm from the laser-plasma axis with a precise xyz-holder. The resolved spectra were monitored using a fast response ICCD camera (type Andor- iStar DH734-18F) and the data acquisition was carried out using KestrelSpec® 3.96 software at a resolution of 0.02 nm per pixel (of size 196 μm^2).

The nano silver was supplied as a powder (MKNano®) with product label MKN-Ag-090 (CAS 7440-22-4), with average size of 90 ± 10 nm. The nano-powder is compressed to circular disk tablets with diameter of 10 mm using a 500 kg/cm^2 mechanical press. The shape of the nanoparticles was investigated with a TEM after compression: almost spherical diameters of 95 ± 15 nm are found, and only slight distortions were observed. Both delay and gate times were adjusted to the levels of 2 μs across the experimental studies. Background stray light during experimental runs was measured and subtracted with the help of Andor iStar ICCD- KestrelSpec® software. The noise level from the detection electronics was recorded across the entire wavelength region (250-850 nm) and was found to be about 20 ± 7 counts. The signal-to-noise ratio was computed using as noise-level the sum of the electronic noise in addition to the continuum emission (sometimes called background radiation) that occurs underneath the atomic lines of interest. The incident laser energy for each laser pulse was measured utilizing a quartz beam splitter. The reflected part (4%) was incident on an absolutely calibrated power-meter (Ophier model 1z02165). The laser pulse shape was measured using a 25 ps, fast-response photodiode in conjunction with a digital storage CRO (type Tektronix model TDS-1012), and the pulse-width was found stable at a level of 5 ± 1 ns. The laser energy was adjusted with a set of calibrated neutral density filters. The absolute sensitivity of the spectrograph, camera and optical fiber was calibrated using a DH2000-CAL lamp (supplied by Ocean Optics-SN: 037990037). The data presented in this article are taken as the average over three consecutive shots onto fresh targets, and the date are presented together with standard deviations about means and plotted as error bars associated with the measurement points. The observed spectral Ag I lines (e.g., 328.02, 338.2, 405.5, 421.2, 447.6, 467.7, 520.9, 546.5, 768.7 and 827.3 nm) were examined in view of self-absorption and/or self-reversal.

4. Results

The spectral emission is recorded in different spectral regions from the plasma that is generated by interaction of high peak power laser radiation using the third harmonic, blue wavelength of 355 nm with silver nano-based targets and the corresponding bulk material. Figure 1 displays the measured data.

Preprints (www.preprints.org) | NOT PEER-REVIEWED | Posted: 1 August 2018 doi:10.20944/preprints201808.0003.v1

Peer-reviewed version available at Atoms 2018, 6, 44; doi:10.3390/atoms6030044

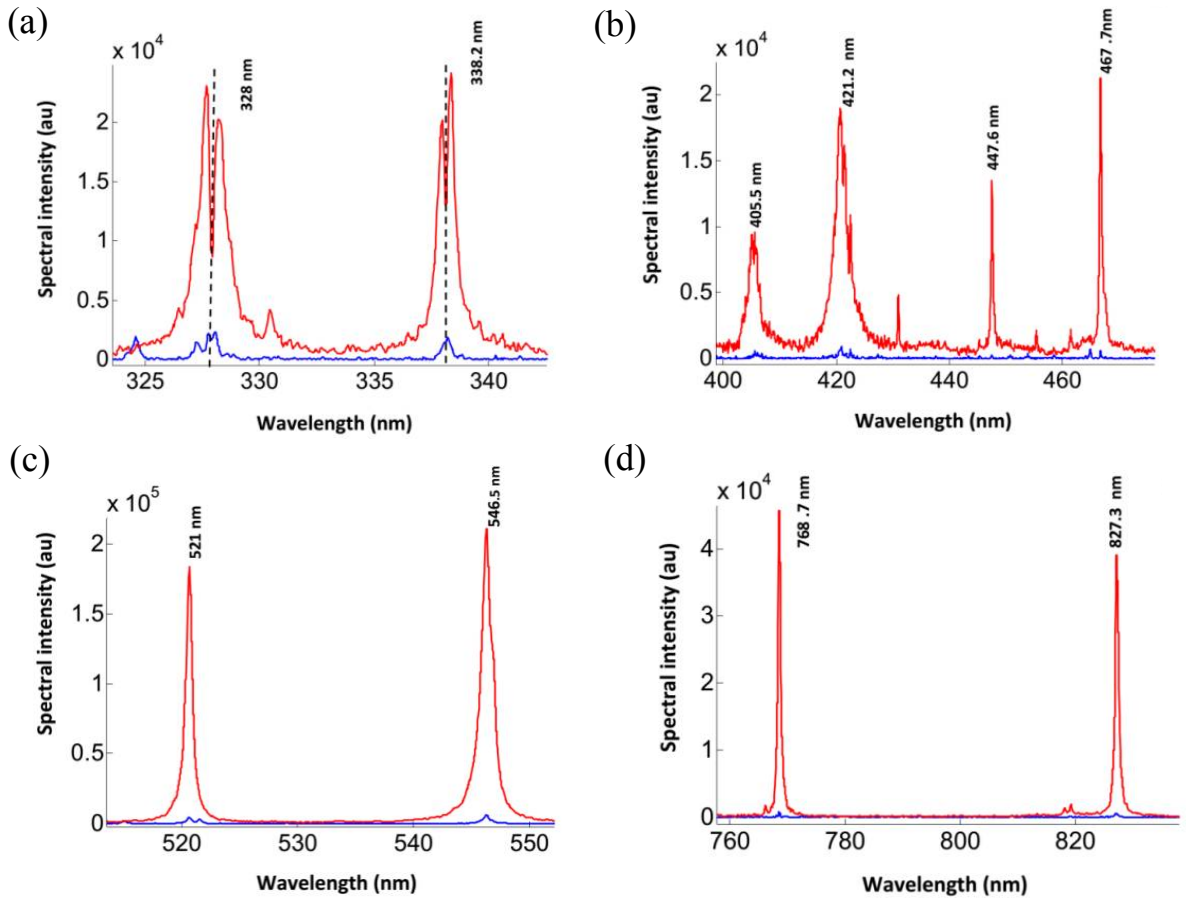

Figure 1. (a) to (d) Emission spectra at different wavelength regions from nano-based silver target (in red) and bulk target plasma (in blue).

There is an obvious larger emission from the nano- based silver plasma than that from plasma created from the bulk target (ratio of the red to blue curves). Detailed inspection of the resonant transitions ***4d*^{10}*5p-4d*^{10}*5s*** at wavelengths of 328.06 nm and 338.28 nm (as depicted in Figure 2) indicates existence of self-reversal as well as self-absorption.

Self-reversal is often associated with the population density of the ground state of the silver atoms (***4d*^{10}*5s-state***). The ground-state population exhibits a strong gradient of the plasma parameters (electron density and temperature) ranging from the plasma core to the periphery [1, 2, 3, 4, 5]. Moreover, this effect was found to be pronounced at shorter wavelength laser irradiation at 355 nm, (see Figure 2(a) - blue curve). This is in contrast to the emission from the bulk-based silver target under similar conditions.

The results are consistent with previous studies [21] that discussed that the population density of the ground state is larger for the plasma created at the surface of the nano-based target than that for bulk-based plasma, described by the enhancement factor that is defined by $\left(Enh.Factor = \frac{I_o^{Nano}}{I_o^{Bulk}} \approx \frac{N_o^{Nano}}{N_o^{Bulk}} \right)$. Here, $\frac{I_o^{Nano}}{I_o^{Bulk}}$ is the ratio of the spectral radiance of nano-based to bulk-based target plasma spectral line. Whereas, $\frac{I_o^{Nano}}{I_o^{Bulk}}$ is the ratio between the corresponding population density of the ground state of the silver atoms. For the quantification of self-absorption and/or self-reversal one should rely on certain optically thin (standard) spectral lines which should allow precise measurements of plasma electron density [29]. The presence of H_α emission spectra provides a good candidate for the measurement of the plasma electron density, but H_α is often absent during the interaction of both green and blue lasers, and therefore, one should consider other

Preprints (www.preprints.org) | NOT PEER-REVIEWED | Posted: 1 August 2018 doi:10.20944/preprints201808.0003.v1

Peer-reviewed version available at Atoms 2018, 6, 44; doi:10.3390/atoms6030044

optically thin lines that can be measured during the interaction of the different Nd:YAG harmonics with nano-based targets.

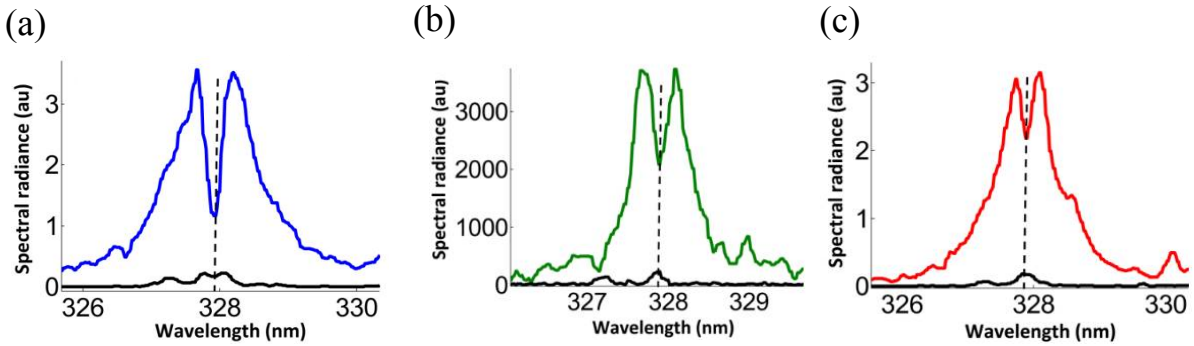

Figure 2. Self-reversal of the resonance Ag I line at wavelength of 328 nm. The colored (larger) spectra from nano-based target plasma and lower black from bulk-silver target at laser irradiation wavelength (a) 355 nm, (b) 532 nm, and (c) 1064 nm.

The Ag I lines at wavelengths of 768.7 and 827.35 nm are candidates for electron density measurements. At the reference density of 1 × 10^{17} cm^{-3}, the Stark broadening parameters of $\omega_S^{827.35} = 0.18(nm)$, $\omega_S^{768.7} = 0.17(nm)$ allow one to estimate electron density from the Lorentzian (FWHM) component of each line. The fitting of the line shapes to Voigt profiles is shown in Figure 3. The overall results are summarized in Table 1, including electron densities measured from the optically thin H_α.

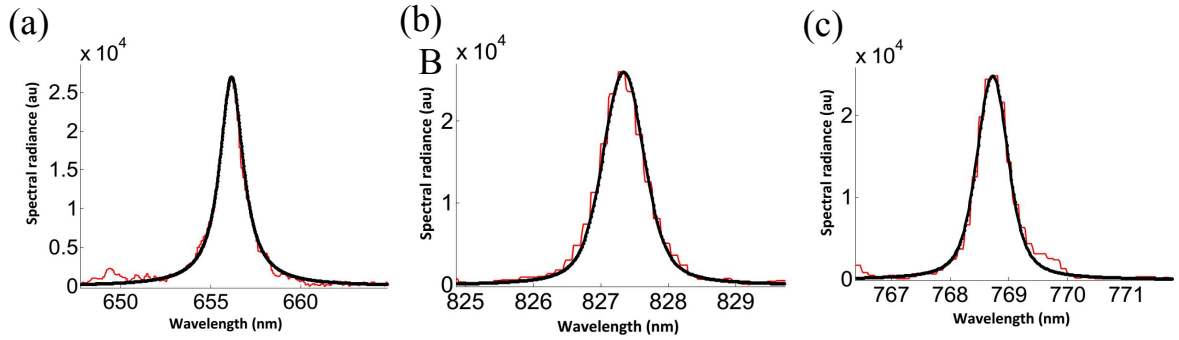

Figure 3. Fitting of line shapes (red) to Voigt line shape (black) for the H_α- line (a) and the Ag I lines at 827.35 (b) and 768.7 nm (c) at fixed laser fluence 9.6 J/cm^2 and IR laser at 1064 nm excitation.

Table 1: Electron densities inferred from different spectral lines.

Laser fluence (J/cm^2)	$n_e(H_\alpha)$ (10^{17} cm^{-3})	n_e Ag I-827.35 nm (10^{17} cm^{-3})	n_e Ag I-768.7 nm (10^{17} cm^{-3})
9.94	**1.64**	**1.66**	**1.76**
7.46	**0.76**	**0.77**	**0.76**
5.9	**0.63**	**0.66**	**0.7**
4.47	**0.57**	**0.55**	**0.58**

The results in Table 1 attest that the two lines at wavelengths of 768.7 and 827.35 nm can be utilized for reliable measurements of plasma electron density at the surface of silver nano-based targets during interaction with the blue, Nd:YAG laser radiation.

This work also explores optical depths of laser-plasma generated with the green and blue wavelengths. In general, the laser produced plasma is inhomogeneous, even though the laser device operates in TEM_{00}-mode [1, 2, 3, 4, 5, 6, 7, 8, 9, 10]. Actually, there are two regions in the plasma produced by laser radiation, first, the central hot core with relatively large electron temperature and density and large population densities of higher emitting species. Second, the outer periphery region at which the plasma becomes relatively cold (losses of internal energy by adiabatic expansion against surrounding medium) [23, 24 , 29]. The second region contain large populations in lower excitation states. This situation enhances the chance or probability for some generated photons at the central region to be re-absorbed by the cold atomic species at the cold peripheries [23, 24].

The re-absorption processes act differently over the spectral line shape. The effect at the central upshifted spectral line with little effect at the line wings is called self-reversal [25, 26, 27], and it produces a dip as indicated in Figure 4. The other re-absorption process is self-absorption. It is difficult to assess the level of self-absorption in n_e determinations but usually larger electron densities are found from self-absorbed lines. Comparisons with well-established, optically thin emission lines can be utilized to evaluate the level of self-absorption. The existence of certain, reliable optically thin lines can provide a measure from which one can deduce if a recorded line is optically thin or thick. Hence, the standard H_α-line or other optically thin lines like the Ag I lines at 768.7 or 827.35 nm become important since one can use either line to check the value of the electron density [29].

Comparisons of the electron densities inferred from questionable lines with n_e obtained from optically thin lines can yield the self-absorption parameter, SA [29], using the following formula $SA \simeq \left(\frac{1-\exp(-\tau_{SA})}{\tau_{SA}} \right)$. Here, $\tau_{SA} \simeq \int_{-\ell}^{0} \kappa_{SA}(\lambda)\, d\lambda$ is the plasma optical depth due to self-absorption coefficient $\kappa_{SA}(\lambda)$ integrated over the whole spectral line region, $\Delta\lambda$, along the line of sight for plasma having approximate length ℓ. This absorption causes an apparent line shape distortion (enlarged FWHM and reduced spectral radiance). It was pointed out in Ref. [29] that a correction to a spectral line shape against self-absorption can be carried out using a practical relation, $SA \simeq \left(n_e^{line} / n_e^{*} \right)^{-1.785}$, where n_e^{*} is the electron density deduced from largely optically thin lines, e.g., H_α at 656.3 nm, Ag I at 768.7 or 827.35 nm, as mentioned before. As the SA parameter approaches unity, the line can be considered as optically thin. In other words, the SA parameter determines the degree of the plasma opacity of selected spectral lines.

Similarly, the self-reversal effect can be quantified with coefficient $SR \simeq \left(\frac{1-\exp(-\tau_{SR})}{\tau_{SR}} \right)$ that can be related to the transmittance $T(\tau_{SR}) \approx \left(1/\sqrt{\pi\tau_{SR}} \right)$ [26, 27] with plasma of optical depth τ_{SR}. The SR parameter, typically not much smaller than one, can cause a characteristic dip at the center of the line, as shown for example in Figures 4 (a) and 4 (b) for the resonance lines Ag I at 328.0 and 338.2 nm, while SR has little effect in the line wings [27].

Peer-reviewed version available at Atoms 2018, 6, 44; doi:10.3390/atoms6030044

For constant fluence of 9.6 J/cm² and for blue laser irradiation, Figures 4 (a) and (b) display self-reversed Ag I resonance lines at wavelengths of 328 and 338.2 nm. Two major features occur: (i) the dip at each of the lines centers, and (ii) the pronounced line asymmetry of both lines.

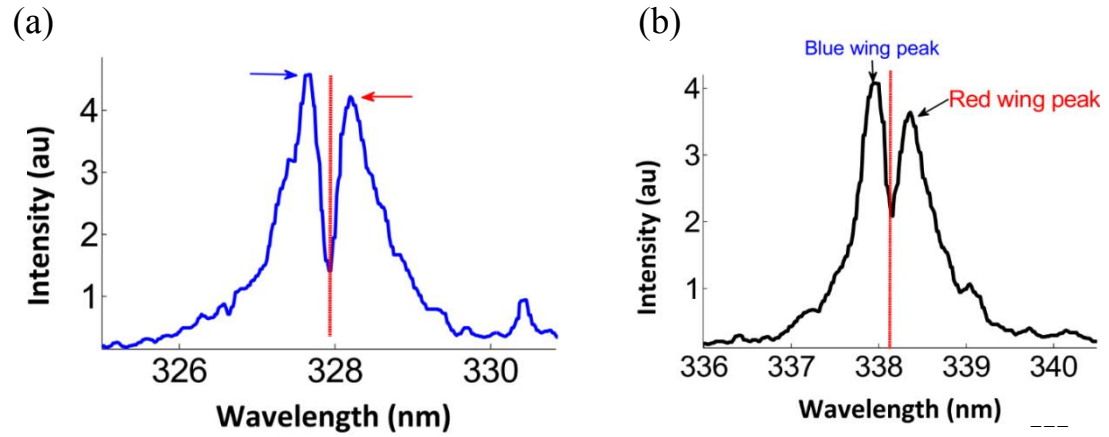

Figure 4. The spectral lines dip to Ag I resonance lines at irradiance level of 9.6 J/cm² with blue laser wavelength with indication to line asymmetry. (a) 328 nm; (b) 338.2 nm.

Notice the asymmetry in the line shapes that appears to affect the red wings of both lines. The theory that can describe the spectral dip due to self-reversal does not contain an asymmetry. However, the apparent asymmetry will be subjected to further investigation in a separate study.

However, in order to retrieve the undistorted line shape by self-reversal, Figure 5 displays results of fitting the measured self-reversed lines (in red) to the "symmetric" transmittance line shape (in black), using $T(\lambda)=\int \varphi(\lambda)\mathrm{e}^{-(\varphi_o\cdot\tau_{\lambda o})}\,d\lambda$ [26, 27] with assumed Lorentzian spectral shape $\varphi(\lambda)=\frac{1}{\pi}\frac{0.5\Delta\lambda_S}{(\lambda-\lambda_o)^2+(0.5\Delta\lambda_S)^2}$, with plasma optical depth that is given by $\tau_{\lambda_o}=\int_{-\ell}^{0}\kappa(\lambda_o)\cdot d\ell$ and line absorption coefficient of $\kappa(\lambda_o)$ at the un-shifted wavelength (λ_o). The indicated fitting procedure yields the distorted FWHM, $\Delta\lambda_{S2}$ (nm).

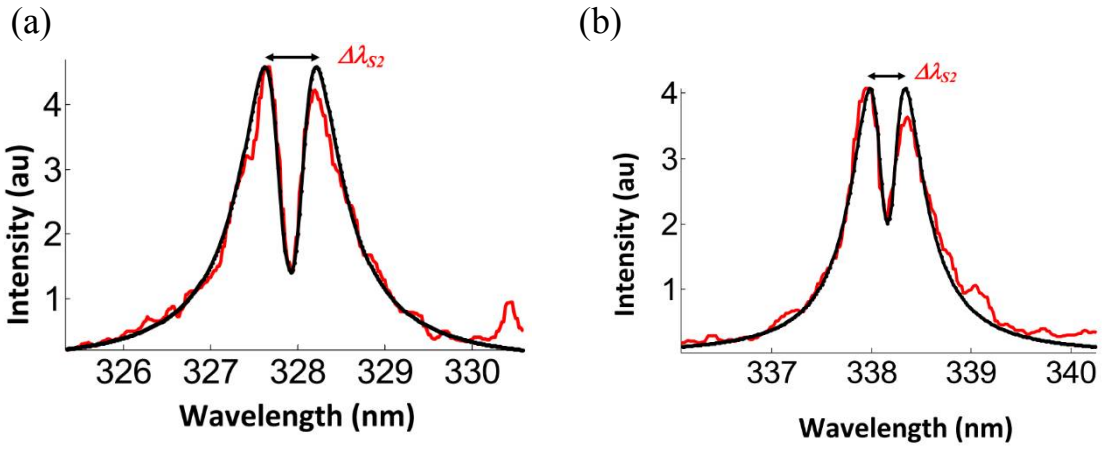

Figure 5. Fitting of the symmetric transmittance function (in black) to measured self-reversed lines (in red) for two silver lines. (a) 328 nm; (b) 338.2 nm.

Preprints (www.preprints.org) | NOT PEER-REVIEWED | Posted: 1 August 2018 doi:10.20944/preprints201808.0003.v1

Peer-reviewed version available at Atoms 2018, 6, 44; doi:10.3390/atoms6030044

Figures 6 (a) and (b) display the results of retrieved (undistorted) Lorentzian line shape of both lines with FWHM - $\Delta\lambda_{s1}$ (nm) that is apparently smaller than $\Delta\lambda_{s2}$ (nm). Hence, one can use $\Delta\lambda_{s1}$ to determine the plasma electron density via relation [28] $\left(\frac{n_e^{line}}{N_r} \simeq \frac{\Delta\lambda_{S1}}{\omega_{line}}\right)$. The electron densities $\left(n_e^{328} \simeq 4.1\times10^{18}\ cm^{-3}\right)$ and $\left(n_e^{338} \simeq 3.2\times10^{18}\ cm^{-3}\right)$, respectively, are significantly larger than the electron density $\left(n_e^{827} \simeq 2.9\times10^{17}\ cm^{-3}\right)$ measured using the optically thin line at 827.4 nm for the same experimental conditions.

Even after the application of the "symmetric" transmittance function, the retrieved FWHM $\Delta\lambda_{s1}$ appears larger than the expected value by more than one order of magnitude, and consequently, one should consider other effects that can lead to further distortion of spectral line shapes.

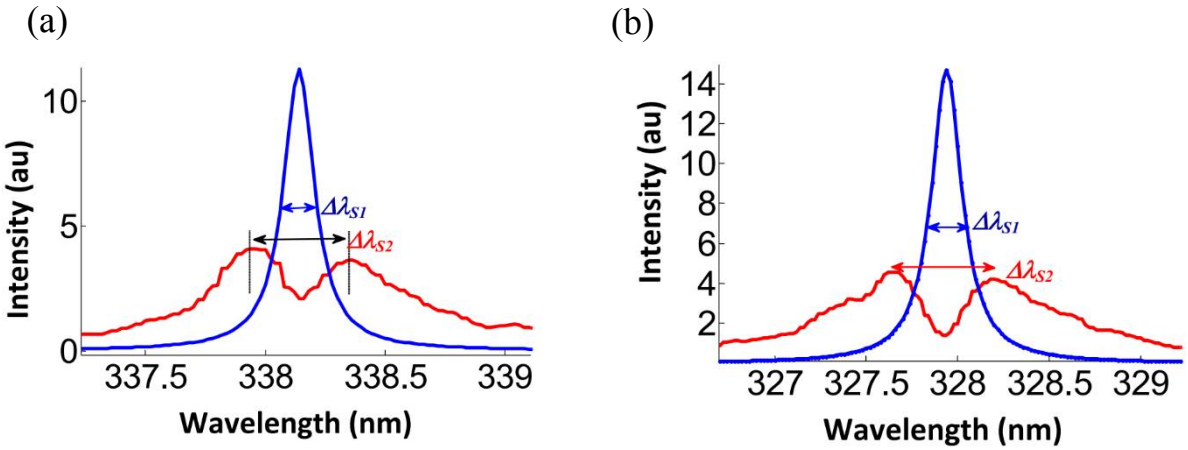

Figure 6. The retrieved line shape after self-reversal effect for two silver lines. (a) 328 nm; (b) 338.2 nm.

The amount of self-absorption can be determined from the coefficient $SA \simeq \left(n_e^{line}/n_e^{827}\right)^{-1.785}$ [29] which shows values of SA << 1, for the two lines respectively, i.e., the plasma that arises from the nano-based silver target is optically thick for the two resonance lines under consideration.

Figure 7 (a) shows spectral line shape of the 327.9 nm resonance line upon the irradiation by the blue laser at different levels of laser fluence.

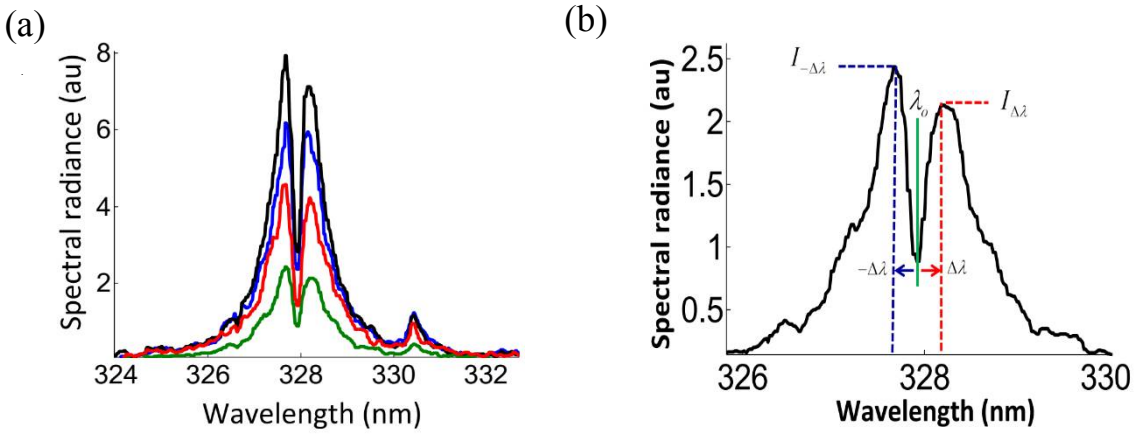

Figure 7. (a) Spectral radiance of the line 327.9 nm with asymmetry for different laser fluence levels. (b) Details for determination of the spectral asymmetry.

Peer-reviewed version available at Atoms 2018, 6, 44; doi:10.3390/atoms6030044

The observed spectral line asymmetry, *As*, that appeared for the 328 nm line can be calculated [4] using $As = 2\left(\frac{I_{\Delta\lambda} - I_{-\Delta\lambda}}{I_{\Delta\lambda} + I_{-\Delta\lambda}}\right) \approx \left(\frac{hc}{\lambda_o kT_R} - 6\right)\frac{2\Delta\lambda}{\lambda_o}$. Here, $I_{\Delta\lambda}$ and $I_{-\Delta\lambda}$ are the peak spectral radiances at red and blue wings as shown in Figure 7(b), T_R is the radiation temperature - not the electron temperature T_e because the laser-induced plasma is in local thermodynamic equilibrium (LTE) which implies that the these temperatures are not equal $T_R \neq T_e$. Table 2 shows the amount of line asymmetry for decreasing laser fluence.

Table 2: Line asymmetries, self-absorption factor, and Keldysh parameters for different fluence.

Fluence (J/cm²)	13.4	10.9	6.9	5.6	4.8	3.9	2.1
Line Asymmetry %	4	5.7	1.2	14	7.1	8.7	11.1
n_e^{827} $(10^{17}\ cm^{-3})$	3.5	3.4	2.2	2	1.33	1.2	1.1
Self-absorption SA	0.01	0.011	0.007	0.0048	0.0044	0.0022	0.0021
Keldysh parameter	473	524	659	732	791	877	1195

5. Discussion

Recent work elaborates on the interaction of the Nd: YAG radiation at wavelengths of 1064, 532 and 355 nm with silver nano-based targets and for different laser fluence levels in the range of 2 to 13 J/cm². Three observations are identified for the resonance lines at 328 and 338.2 nm, and investigations of the spectral lines shapes reveal:

(I) Self-reversal as characterized by large dip at the central wavelength [30];

(II) Self-absorption; and

(III) Asymmetries.

In the previously reported experiments, there was no recognizable trend of the line asymmetry variation with either laser fluence or electron density. However, for an explanation of the observed phenomena, one should consider effects associated with internally generated micro electro-magnetic fields [4, 5, 6, 7, 30].

In addition, the spectral lines arise from the Ag I at the wavelengths of 768.7 and 827.35 nm are found to be optically thin when comparing the measured electron density to that obtained from H_α. Consequently, these two Ag I lines can be used as a standard spectral line to measure the plasma electron density in case of absence of H_α.

6. Conclusions

The emitted resonance spectral lines in nano-enhanced laser-induced plasma spectroscopy indicate self-reversal and asymmetries. Possibly, effects from the plasma internal electro-magnetic fields may cause the observed line asymmetry. Further experimental and theoretical efforts are recommended for the explanation of the spectral line shapes from the nano-material plasma. Several lines at near-IR wavelengths are optically thin, and these lines can be used as a reliable indicator of plasma electron density.

Author Contributions: Ashraf M. EL Sherbini designed and performed the experiments. Ashraf M. EL Sherbini and Ahmed E. EL Sherbini analyzed the result together with Christian G. Parigger, and all three authors contributed to the writing of the article.

Conflicts of Interest: The authors declare no conflict of interest.

References

1. Cremers, D.A. Radziemski, L.J. *Handbook of Laser-Induced Breakdown Spectroscopy*; Wiley: Hoboken, NJ, USA, **2006**; ISBN: 978-0-470-09299-6.
2. Radziemski, L.J., Solarz, R.W., Paisner, J.A., Eds. Laser Spectroscopy and its Applications, Marcel Dekker: New York, NY, USA, **1987**, ISBN: 978-0824775254.
3. Parigger, C.G. Laser-induced breakdown in gases: Experiments and simulation. In *Laser-induced breakdown spectroscopy*. Miziolek, A. W., Palleschi, V., and Schechter, I., Eds. Cambridge University Press: Cambridge, UK, **2006**; ISBN: 978-0521852746.
4. Griem H. R. *Plasma Spectroscopy*; McGraw-Hill Book Company: New York, NY, USA, **1964;** LCCN 63023250
5. Fujimoto T. *Plasma Spectroscopy*; Clarendon Press: Oxford, UK, **2004**; ISBN: 9780198530282.
6. Kunze H.-J. *Introduction to Plasma Spectroscopy*; Springer: New York, NY, USA, **2009**; ISBN: 978-3-642-02232-6
7. Lochte-Holtgreven W., Ed. *Plasma Diagnostics*; Wiley: North-Holland, Amsterdam, NL, **1968**; ISBN: 978-0720401370.
8. EL Sherbini, A. M., Aboulfotouh, A. M., Parigger, C. G. Electron number density measurements using laser-induced breakdown spectroscopy of ionized nitrogen spectral lines. *Spectrochim. Acta Part B: At. Spectrosc.* **2016**, 125, pp. 152–158; doi: https://doi.org/10.1016/j.sab.2016.10.003.
9. Oks, E. *Stark Broadening of Hydrogen and Hydrogen Like Spectral Lines on Plasmas: The Physical Insight*; Alpha Science International: Oxford, UK, **2006**; ISBN: 1-84265-252-4.
10. Parigger CG, Plemmons DH, Oks E. Balmer series Hβ measurements in a laser-induced hydrogen plasma. *Appl. Opt.* **2003**, 42, pp. 5992–6000; doi: https://doi.org/10.1364/AO.42.005992.
11. Oks, E. The Shape of Spectral Lines of Two-Electron Rydberg Atoms/Ions: Analytical Solution; *J. Phys. B: At. Mol. Opt. Phys.* **2017**, 50, 115001; doi: https://doi.org/10.1088/1361-6455/aa66c4.
12. Pokropivny, V., Lohmus, R., Hussainova, I., Pokropivny, A., Vlassov, S. *Introduction in nanomaterials and nanotechnology*. University of Tartu, Tartu Press: Tartu, FI, **2007**; ISBN: 978-9949-11-741-3
13. Marambio-Jones, C., Hoek, E. M. V. A review of the antibacterial effects of silver nanomaterials and potential implications for human health and the environment. *J. Nanopart. Res.* **2010**, 12, pp. 1531–1551; doi: https://doi.org/10.1007/s11051-010-9900-y.
14. Campillo, I., Guerrero, A., Dolado, J.S., Porro, A., Ibáñez, S.Goñi A. Improvement of initial mechanical strength by nanoalumina in belite cements. *Materials Lett.* **2007**, 61, pp. 1889-1892; doi: https://doi.org/10.1016/j.matlet.2006.07.150.
15. Yurkov, G. Yu. Fionov, A. S. Koksharov, Yu. A. V., Koleso, V., Gubin, S. P. Electrical and magnetic properties of nanomaterials containing iron or cobalt nanoparticles. *Inorganic Materials* **2007**, 43, pp. 834–844; doi: https://doi.org/10.1134/S002016850.
16. Ray, P. C. Size and Shape Dependent Second Order Nonlinear Optical Properties of Nanomaterials and Their Application in Biological and Chemical Sensing. *Chem. Rev.* **2010**, 110, pp. 5332-5365; doi: https://doi.org/10.1021/cr900335q.

17. Yang, H., Liu, C., Yang, D., Zhang, H., Xi, Z. Comparative study of cytotoxicity, oxidative stress and genotoxicity induced by four typical nanomaterials: the role of particle size, shape and composition. *J. Appl. Toxicol.* **2009**, 29, pp. 69–78; doi: https://doi.org/10.1002/jat.1385.
18. Ohta, T., Ito, M., Kotani, T., Hattoti, T., Emission enhancement of laser-induced breakdown spectroscopy by localized surface plasmon resonance for analyzing plant nutrients. *Appl. Spectrosc.* **2009**, 63, pp. 555–558; doi: https://doi.org/10.1366/000370209788346896.
19. EL Sherbini, A.M., Aboulfotouh, A.-N.M., Rashid, F., Allam, S., EL Dakrouri, T.A. Observed enhancement in LIBS signals from Nano vs. Bulk ZnO targets: Comparative study of plasma parameters. *World J. Nanosci. Eng.* **2012**, 2, pp. 181–188; doi: https://doi.org/10.4236/wjnse.2012.24024.
20. EL Sherbini, A.M., Galil, A.A., Allam, S., EL Sherbini, Th.M. Nanomaterials induced plasma spectroscopy. J. Phys.: Conf. Ser. **2014**, 548, 012031.
21. EL Sherbini, A.M., Parigger, C.G, Wavelength dependency and threshold measurements for nanoparticle-enhanced laser-induced breakdown spectroscopy. *Spectrochim. Acta B: At. Spectrosc.* **2016**, 116, pp. 8–15; doi: https://doi.org/10.1016/j.sab.2015.11.006.
22. EL Sherbini, A.M., Parigger, C.G. Nano-material size dependent laser-plasma thresholds. *Spectrochim. Acta Part B: At. Spectrosc.* 2016, 124, pp. 79-81; doi: https://doi.org/10.1016/j.sab.2016.08.015.
23. Mulser, P., Bauer, D. *High Power Laser–Matter Interaction*; Springer Verlag: Heidelberg, DE, **2010**; ISBN: 978-3-540-46065-7.
24. Hahn, D., Omenetto, N. Laser-induced breakdown spectroscopy (LIBS), part II: review of instrumental and methodological approaches to material analysis and applications to different fields, *Appl. Spectrosc.* **2012**, 66, pp. 347–419; doi: https://doi.org/10.1366/11-06574.
25. Holstein, T. Imprisonment of Resonance Radiation in Gases. *Phys. Rev.* **1947**, 72, pp. 1212-1233; doi: https://doi.org/10.1103/PhysRev.72.1212.
26. Holstein, T. Imprisonment of Resonance Radiation in Gases. II. *Phys. Rev.* **1951**, 83, pp. 1159-1168; doi: https://doi.org/10.1103/PhysRev.83.1159.
27. Irons, F.E. The escape factor in plasma spectroscopy—I. The escape factor defined and evaluated. *J. Quant. Spectrosc. Radiat. Transfer* **1979**, 22, pp. 1-20; doi: https://doi.org/10.1016/0022-4073(79)90102-X.
28. Konjević, N. Plasma Broadening and Shifting of Non-Hydrogenic Spectral Lines: Present States and Applications. Physics Reports **1999**, 316, pp. 339-401; doi: https://doi.org/10.1016/S0370-1573(98)00132-X.
29. El Sherbini A.M., El Sherbini T.M., Hegazy H., Cristoforetti G., Legnaioli S., Palleschi V., Pardini, L., Salvetti, A., Tognoni, E. Evaluation of self-absorption coefficients of aluminum emission lines in laser-induced breakdown spectroscopy measurements. *Spectrochim. Acta Part B: At. Spectrosc.* **2005**, 60, pp. 1573–1579; doi: https://doi.org/10.1016/j.sab.2005.10.011.
30. Hey, J. D., Korten, M., Lie, Y., Pospieszczyk, T., Rusbüldt, A., Schweer, B., Unterberg, B., Wienbeck, J., Hintz, E. Doppler Broadening and Magnetic Field Effects on the Balmer Lines Emitted at the Edge of a Tokamak Plasma. Contrib. Plasm. Phys. **1996**, 36, pp. 583-604; doi: https://doi.org/10.1002/ctpp.2150360505.